Available online at www.sciencedirect.com

ScienceDirect

Energy Procedia 67 (2015) 31 – 42

Energy Procedia

5th Workshop on Metallization for Crystalline Silicon Solar Cells

Combined microstructural and electrical characterization of metallization layers in industrial solar cells

P. Kumar[a], B. Willsch[a], M. Dürrschnabel[a], Z. Aabdin[a], R. Hoenig[b], N. Peranio[a], F.Clement[b], D. Biro[b], O. Eibl[a,*]

[a]*Eberhard Karls University of Tuebingen, Institute of Applied Physics, Auf der Morgenstelle 10, 72076 Tuebingen, Germany*
[b]*Fraunhofer Institute for Solar Energy Systems (ISE), Heidenhofstr. 2, 79110 Freiburg, Germany*

Abstract

Screen printed front side contacts of textured, mono-crystalline p-type silicon solar cells with n-type emitters were investigated. The different pastes (FSP1 and 2) and the different crystallographic orientations of the Si surfaces studied strongly affected the contact resistance. The microstructure of the contacts was analyzed in plan-view and cross-section by combined scanning and analytical transmission electron microscopy. A controlled grinding process rather than a chemical etching process was applied for the plan-view sample preparation. For textured cells processed with different pastes, pronounced differences were seen in the contact resistances (FSP1: efficiency 16.9% and contact resistance 20 mΩ cm^2, FSP2: 17.8% and < 5 mΩ cm^2). A discontinuous glass layer was found for FSP1 but a continuous glass layer was found for FSP2, yielding a smaller contact resistance. Glass layers contained $(Si_2Pb)O_x$ as a main constituent but different mole fractions of Zn, Ti, P, and B as minor constituents, varying for the different pastes. Glass layers were up to 500 nm thick and revealed inhomogeneously distributed spherical Ag colloids 5-200 nm in size. Planar cells were also studied and served as model systems: planar ⟨111⟩ oriented Si surfaces yielded specifically lower contact resistance as compared to planar ⟨100⟩ orientation. Pyramidal Ag crystallites were only observed for ⟨100⟩ oriented Si surfaces not for ⟨111⟩ surfaces. Therefore, it is concluded that pyramidal Ag crystallites are not necessary for contacts yielding low contact resistance. Instead, lens shaped Ag precipitates together with a high density of Ag colloids in the glass layer yield low contact resistance, as found for <111> oriented Si surfaces. A percolative current path including charge transport via Ag colloids in the glass layer is proposed. For textured cells, in accordance with these results, pyramidal Ag crystallites were only observed at step edges of {111} faces or at the edges of the Si pyramids.

Peer-review under the responsibility of Gunnar Schubert, Guy Beaucarne and Jaap Hoornstra

Keywords: crystalline silicon solar cells; metallization; screen printing; contact formation

* Corresponding author. Tel.: +49 7971 29 76346; fax: +49 7971 29 5093.
E-mail address: oliver.eibl@uni-tuebingen.de

Peer-review under the responsibility of Gunnar Schubert, Guy Beaucarne and Jaap Hoornstra
doi:10.1016/j.egypro.2015.03.285

1. Introduction

Understanding the role of screen printed front side contacts is one of the main challenges for improving the contacting of mono-crystalline p-type silicon solar cells with n-type emitters. The research project *MikroSol* dealt with these issues and first results were published in Ref. [1], more detailed results are reported in this paper. Within the *MikroSol* project a series of more than 2000 solar cells were produced, planar (shiny etched) and textured cells, Si wafers with <100> and <111> orientation and processed with different pastes. The influence of paste composition, firing process, and role of gas ambient annealing on the performance of cells is well understood in literature [2–5]. However, there is still ambiguity about the influence of crystallographic orientation on the microstructural features at silicon metallization interface (SMI) and its correlation to the contact resistance of the cells.

Commercially available front side pastes typically consist of silver powders, glass frits, and some organic binders. The main task of the glass frits is to etch through the antireflection coating (usually SiN_x), enabling an electrical contact to the emitter of the solar cell [6]. The paste yields a complex silicon metallization interface including an interfacial glass layer, spherical Ag colloids in the glass layer and pyramidal Ag crystallites penetrating the Si emitter, yielding different opportunities for the resulting current paths. Other important factors for the resulting microstructure are the exact chemical composition of the paste, the processing parameters, and the crystallographic orientation of the Si surfaces.

With respect to the current paths, different hypothesis exist in literature, which are still under debate and were reviewed by Schubert et al. [6]. Two different models were proposed:

- A non-uniform conduction in which current flow occurs via a few Ag crystallites that are possibly in direct contact between the emitter and silver bulk as reported earlier by Ballif et al. and Kontermann et al. [7, 8]
- Current flow through the thin interfacial glass layer richly decorated with nano-Ag colloids as reported by Li et al. and Cho et al. [9, 3]

The electrical conductivity of the glass layer determines whether the electrical transport would be percolative or tunneling. If the ratio of conductivities ($\sigma_{insulator}/\sigma_{conductor}$) is very small in the conductor-insulator systems then such systems are best described by the percolation theory [10]. A review on percolative systems was given in Ref. [11]. Since in the glass layer the distance between metallic particles (Ag colloids) is much larger than the tunneling range, the transport mechanism has to be considered as percolative rather than tunneling [12].

Only few papers presented contact resistance measurements together with microstructural analysis, in which special attention was given to the properties of the glass layer [3]. In this paper we summarized a detailed microstructural analysis of textured and planar cells focusing mainly on the contact region (SMI) and its correlation to the contact resistances. Textured cells were investigated contacted with pastes of different chemical composition and, in addition, cells with planar Si surfaces of different crystallographic orientations (⟨100⟩ and ⟨111⟩) serve as model systems. Microstructure was investigated according to the following points:

- Presence of SiN_x layer
- Wetting behavior of the glass phase, chemical composition and thickness of the glass phase.
- Ag crystallites at the SMI, their size and density.
- Ag colloids dispersed in the glass phase at the SMI, their size and density.
- Influence of crystallographic orientation on the morphology of Ag crystallites.
- Microstructure affecting on the contact resistance of the cells.

The influence of the used pastes (FSP1 and FSP2) and the crystallographic orientation of the Si surfaces on the contact resistance were investigated.

A combined scanning electron microscopy (SEM) and transmission electron microscopy (TEM) analysis was applied to analyze the microstructure of the contact region. The contact region, i.e. the Si-metallization interface, affects both the emitter and the space charge region of the solar cell because of diffusion during the heat treatment at elevated temperature [13]. The applied pastes forming the metallic contact contain at least 5 different chemical

elements; therefore, chemical analysis of the samples is of fundamental importance. The standard method for doing this is energy-dispersive X-ray (EDX) spectroscopy in the SEM and TEM. The EDX method, however, is very efficient for the analysis of the contact area but is not able to probe the relevant doping and impurity level in Si due to its detection limits. Therefore, a possible contamination of the Si by elements diffusing from the metallization layer cannot be detected by this method. As a consequence, the microstructural analysis by SEM and TEM can be applied to the contact region, but does not yield significant results for the emitter and space charge region. Therefore, a combination of microstructural analysis with detailed temperature dependent electrical measurements appeared to be urgent.

The results of the electrical measurements of the same solar cells acquired in an optical cryostat in the temperature range between 80 K and room temperature are summarized in the second paper [14]. These results yield significant new insights for the structure-property-correlation of metallic contacts in Si solar cells.

2. Experimental

2.1. Preparation of solar cells with different pastes and differently oriented Si wafers

Solar cells of two different geometries (i) textured and (ii) planar were investigated in this paper (Table 1). For textured samples, H-pattern Al-BSF solar cells were processed using p-type Cz-Si wafers. Planar samples were processed on Si wafers grown by the float zone method. Details of the emitter processing and SiN_x passivation and antireflection coating were described elsewhere [1, 13]. The cells investigated here were processed with different pastes delivered by two different suppliers: paste FSP1 from supplier 1 and pastes FSP2 and FSP3 with similar chemical composition from supplier 2, with paste FSP3 being a newer version of paste FSP2.

For commercial textured cells with ⟨100⟩ oriented Cz-Si wafers, H-pattern metallization of the front side was mainly realized by screen printing of two different commercially available front side pastes FSP1 and FSP2. Both pastes are based on silver as the conducting component. Rapid thermal firing was carried out in an industrial conveyor belt furnace (fast firing oven FFO) at the optimum set point peak firing temperature T_{FFO} given in the Table 1.

Planar cells served as a model system for correlating the microstructural features of the cells with pastes and the substrate orientation. First, two different pastes FSP1and FSP3 were used to contact ⟨100⟩ oriented FZ-Si wafers. Secondly, paste FSP3 was used to contact ⟨100⟩ and ⟨111⟩ oriented FZ-Si wafers. The set point peak firing temperature T_{FFO} is given in Table 1.

2.2. Electrical characterization of large and small-sized cells

The electrical characterization of large cells (15.6×15.6 cm^2) was done with a commercial solar cell tester at the Fraunhofer Institute for Solar Energy Systems (ISE), details are given in Ref. [13]. With these measurements the I-V curve of the large cell was obtained, which yielded the efficiency (η), parallel resistance R_p, series resistance R_s and various other parameters presented in [13]. In addition, transmission line model (TLM) measurements were carried out yielding the specific contact resistance (ρ_c) and other parameters presented in [13].

Within this work, smaller size cells (1×1 cm^2) were then cut out from the large cells and forwarded to the electrical and microstructural characterization (Fig. 1). The small-sample electrical measurements yielded (i) I-V curves under dark and illuminated conditions and, in particular, (ii) the spread of electrical data within one large cell. The small-sized cells were also used for electrical measurements in an optical cryostat at temperatures between 80 K to room temperature [14]. Microstructural analysis was carried out as described below. I-V measurements were interpreted in terms of the two diode model and temperature dependent measurements yielded significant insights. Parallel and series resistances are the most important parameters for correlating the electrical properties and the microstructural features of the cells processed with different pastes.

2.3. Preparation of small-sized cells and microstructural characterization by SEM and TEM

Fig. 1 illustrates the sequence of electrical characterization, advanced preparation and microstructural investigations of the small-sized cells (1×1 cm^2). The electrical characterization was described above. For preparation, advanced techniques were used to achieve high quality electron microscopy images and chemical analysis. For microstructural analysis, various SEM and analytical TEM methods were used to analyze microstructural features at the silicon metallization interface (SMI).

Fig. 2a shows the basic steps for a plan-view and cross-sectional preparation of the textured solar cells. Plan-view samples were prepared by polishing the front side silver contact until the surface fraction covered by the Si pyramids yielded 50% (see Fig. 2a). Note that the Ag metallization finger has a thickness of only 20 µm which requires a careful polishing with fine grain diamond lapping films. For cross-sectional sample preparation a Si dummy was glued on the polished front side of the cell and was then polished in a direction parallel to the metallization finger. The polishing was controlled by a light microscope (see Fig. 2c). Finally, the samples were ion etched to get clean surfaces and forwarded to microstructural analysis by SEM and TEM. For each sample more than 6 areas were investigated.

All plan-view and cross-sectional samples were analyzed in a Jeol 6500F SEM equipped with an Oxford Pentafet EDX detector. An electron energy of 5 keV was chosen to keep the lateral resolution in both backscattered electron (BSE) imaging and EDX spectroscopy as small as possible. Additionally, all relevant characteristic X-ray lines could still be excited and be used for qualitative chemical analysis. In BSE images the resulting grey value of each phase depends on its mean atomic number. For better visualization of the different phases at the SMI, gray scale BSE images were converted into false colored images (see Fig. 2b). High-resolution secondary electron (SE) images were used to image nano-particles at the Si-metallization interface. EDX point spectra were acquired to identify the various phases, 20×20 µm² EDX area scans were acquired to characterize the contacting behavior on the µm level.

Textured plan-view samples contacted with two different pastes FSP1 and FSP2 were investigated by an analytical TEM Zeiss 912 Omega operated at 120 kV. The TEM is equipped with an EDX detector and a low-background specimen holder for chemical analysis with an energy resolution of 136 eV at the Mn-K_α line. The in-column Omega energy-filter was used for acquisition of energy filtered TEM images (EF-TEM) and electron energy-loss spectra (EELS) [1]. The different phases visualized by different colors in the RGB EF-TEM images were identified by TEM-EDX point spectroscopy. All EDX spectra were acquired with a spot size of 32 nm and an acquisition time of 300 s with a stray aperture inserted to avoid stray radiation and to improve the detection limit.

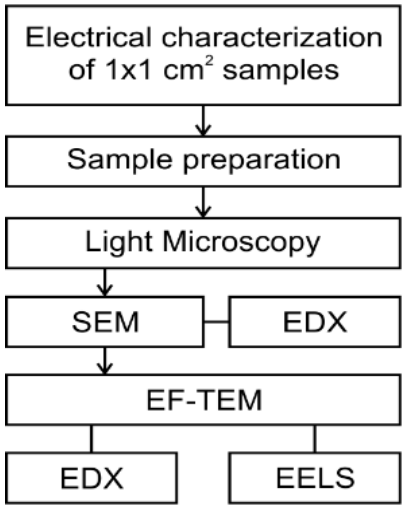

Fig. 1. Flow chart illustrating the sequence of investigations of the electrical and microstructural properties of small size solar cells (1×1 cm^2).

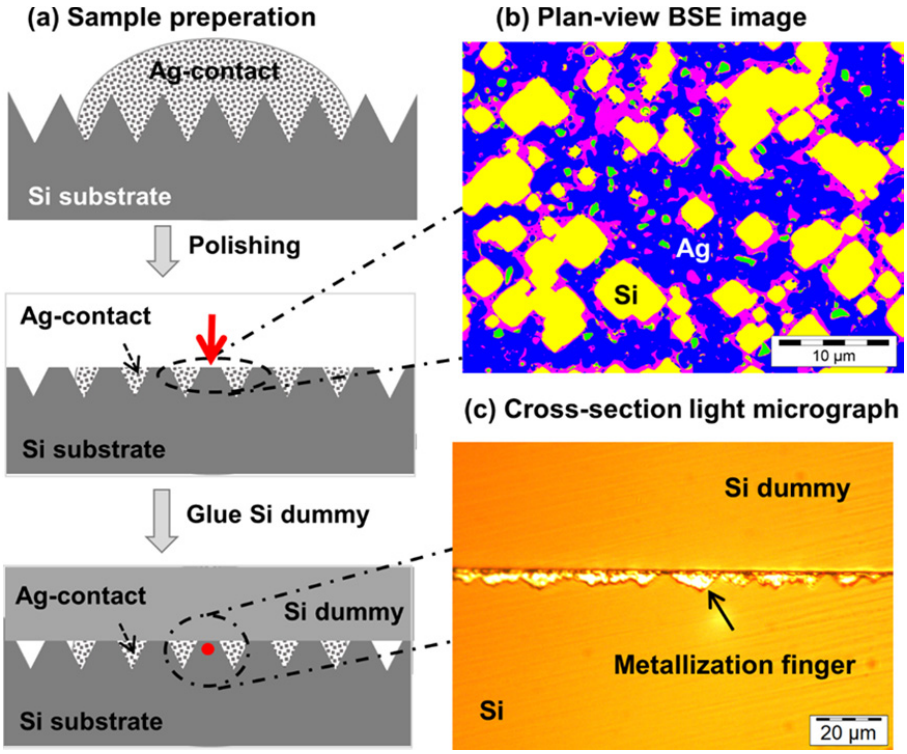

Fig. 2. (a) Flow chart for plan-view and cross-section preparation of textured solar cells. Directions for polishing and view of sight are indicated by red arrows. (b) Plan-view BSE image of the silicon metallization interface (SMI) presented in false colors. (c) Cross-sectional light micrograph of SMI.

3. Results

3.1. Electrical properties of the investigated solar cells

Within the *MikroSol* project a series of solar cells were produced, textured and planar cells, Si wafers with ⟨100⟩ and ⟨111⟩ orientation and contacted with different commercially available pastes referred to as FSP1, FSP2 and FSP3. The sample series included more than 2000 cells. The electrical measurements on these large cells were done with a commercial solar cell tester at Fraunhofer ISE and the specific contact resistances are summarized in Fig. 3. The values were found to be up to 120 mΩ cm^2. Error bars indicate the scatter of data found within a batch of solar cells produced on wafers with same orientation and contacted with the same paste. Planar samples are referred to as shiny etched samples in Fig. 3. The overall finding is that paste FSP1 yielded about 4 times higher contact resistances as compared to other pastes. Planar samples with ⟨111⟩ orientation revealed remarkably 4-8 times lower contact resistance than planar samples with ⟨100⟩ orientation.

Out of 2000 cells processed within the *MikroSol* project only a few representative cells were selected with pronounced differences in contact resistance, efficiencies and, presumably, pronounced differences of the microstructure at the SMI. Processing parameters and electrical properties of the cells are shown in Table 1.

- Textured Cz grown ⟨100⟩ Si wafers were processed at a fixed firing temperature T_{FF0} of 900 °C. The efficiencies of the cells were found in a range between 16.9 to 18 %. Paste FSP1 (sample #T1) yielded a 4 times higher contact resistance but 8 times lower parallel resistance as compared to paste FSP2 (samples #T2 and #T3), see Table 1.
- Planar FZ grown ⟨100⟩ Si wafers were processed at a fixed firing temperature T_{FF0} of 930 °C. In contrast to ⟨100⟩ oriented planar samples, paste FSP1 yielded 2 times lower efficiency as compared to FSP3 (samples #P1 and #P2), see Table 1.
- Planar ⟨111⟩ oriented Si wafers (sample #P3) showed significantly lower contact resistance than cells grown on ⟨100⟩ Si wafers (sample #P2), see Table 1.

The samples shown in Table 1 were forwarded to a microstructural analysis and will be correlated with their electrical properties.

Table 1. Process parameters of textured and planar solar cells as well as electrical data obtained on full size (15.6×15.6 cm^2) cells using the TLM method and I-V characterization with commercial solar cell tester: firing temperature T_{FFO}, efficiency η, specific contact resistance ρ_c, parallel R_p and series resistance R_s.

Geometry	Samples	Substrate	Paste	T_{FF0} (°C)	η (%)	ρ_c (mΩ cm^2)	R_p (Ω cm^2)	R_s (Ω cm^2)
Textured	#T1 (2129)	Cz-Si ⟨100⟩	FSP1	900	16.9	21	4451	0.90
	#T2 (2017)	Cz-Si ⟨100⟩	FSP2	900	17.8	4.7	35506	0.74
	#T3 (1004)	Cz-Si ⟨100⟩	FSP2	900	18.0	5	32123	0.61
Planar	#P1 (1236)	Fz-Si ⟨100⟩	FSP1	930	7.8	33		
	#P2 (1204)	Fz-Si ⟨100⟩	FSP3	930	16.1	11.3		
	#P3 (1111)	Fz-Si ⟨111⟩	FSP3	930	17.1	4.9		

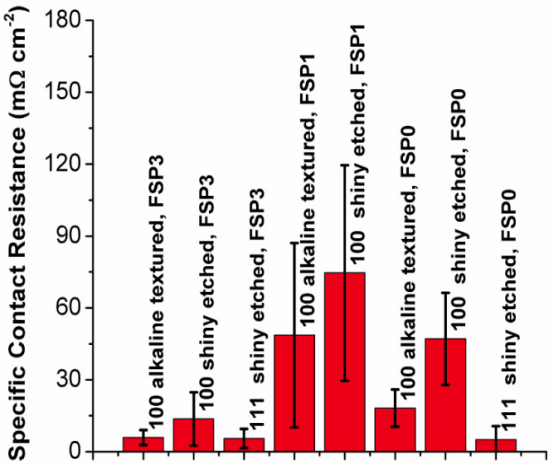

Fig. 3. Specific contact resistance for planar and textured cells using ⟨100⟩ and ⟨111⟩ oriented Si wafers and contacted with different pastes FSP0, FSP1 and FSP3 used within the *MikroSol* project.

3.2. Microstructural analysis of the silicon metallization interface

3.2.1. Textured samples

Textured samples that were partially described in Ref. [1] were analyzed here in more detail by combined SEM and analytical TEM techniques. The previously published results clearly showed the impact of the different pastes on the microstructure of the front side silver contacts, particularly the contact resistance of the cells.

The microstructure and chemical composition of the glass phase in textured cells contacted with paste FSP1 (sample #T1) and paste FSP2 (sample #T2) were analyzed by SEM and analytical TEM (Fig. 4). Fig. (4a and b) show SEM images of the SMI in textured samples for both pastes. Paste FSP1 yielded a high contact resistance (Table 2), a discontinuous wetting of the Si pyramids by the glass phase (Fig. 4a, b), and a low density of Ag colloids dispersed in the glass layer [1]. In contrast, paste FSP2 yielded a low contact resistance, a continuous wetting of the Si pyramids by the glass phase, and a high density of Ag colloids. Further details of the microstructure of the glass layers and Ag colloids are given in Table 2.

Energy-filtered plan-view TEM imaging revealed Ag colloids being smallest in size close to the SMI [1]. The density of Ag colloids close to the SiN_x layer was found to be markedly larger than at areas without a SiN_x layer. A small diameter and a large density of the colloids yield a larger surface on which percolative charge transport might occur [10–12].

The chemical composition of the glass phases obtained from pastes FSP1 and FSP2 were quantitatively analyzed by EDX point spectroscopy in the TEM (Fig. 4c and d). For that, 5-20 spectra were acquired in each sample. Both pastes yielded a glass layer which can be understood as a $(Pb, Si)O_x$ phase with a mole fraction ratio of Si to Pb being close to 2 (Table 3). This might yield additional metallic Pb precipitates [4–6] in the glass layer for a percolative charge transport. As most abundant additives Zn, Ti, and Ag were found, their mole fractions were about a few at%. A logarithmic scale was used to emphasize the small peaks of the additives. For paste FSP1 the Zn and Ti mole fractions are considerably higher as obtained with paste FSP2. Note the differences in the Zn and Ti peaks heights in the EDX spectra (Fig. 4c and d).

Sample #T3 was also contacted with paste FSP2. Therefore, this sample also yielded a low contact resistance, a continuous wetting glass layer on the Si pyramids, and a large density of Ag colloids in the glass layer (Table 2, Fig. 5a). For this sample, the influence of the crystallographic orientation of the faces of Si pyramids on the formation of pyramidal Ag crystallites was investigated. Fig. 5b is a secondary electron (SE) image at larger magnification obtained in the red encircled area in the BSE images shown in Fig. 5a. Lens shaped Ag crystallites were found at {111} faces of the Si pyramids (Fig. 5b), whereas pyramidal Ag crystallites were only found at the edges of the Si pyramids (encircled pyramidal Ag crystallite in Fig. 5b); i.e., the pyramidal Ag crystallites were formed at the intersection of two {111} faces of the pyramids (Fig. 5c). We always observed a glass layer between Ag crystallites and Ag bulk of the finger with a thickness down to 10-20 nm. Hence, we could not directly confirm a current path from the Si emitter to the Ag bulk via the Ag crystallites.

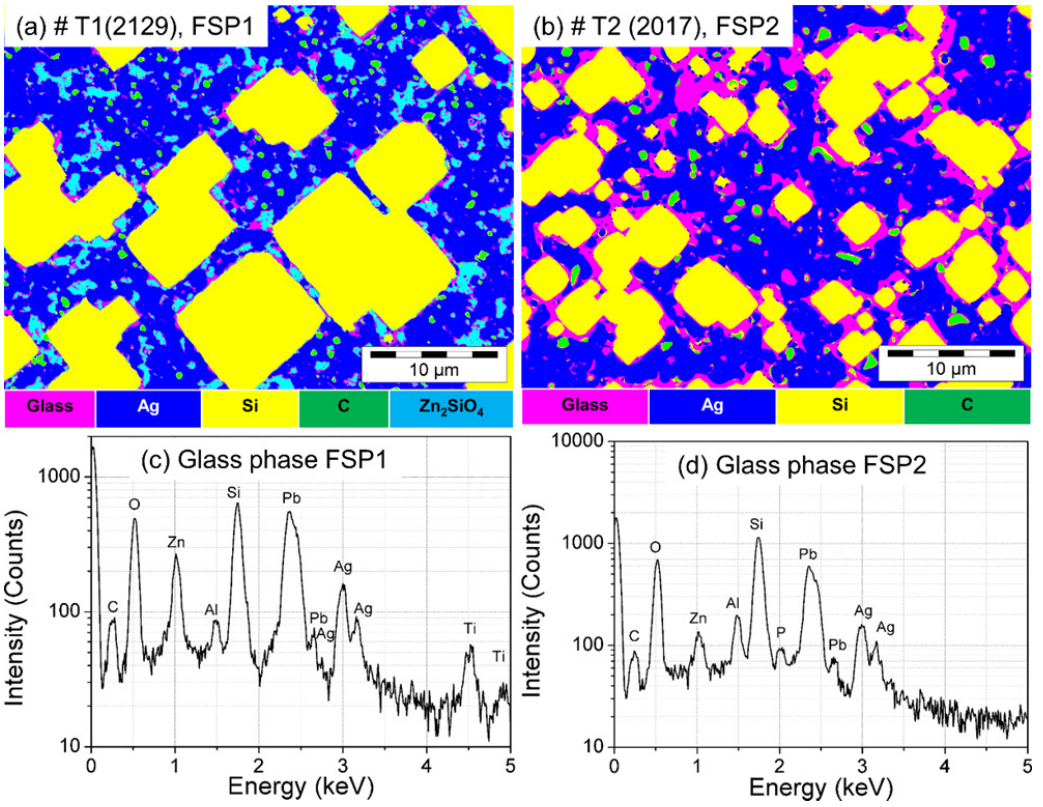

Fig. 4. Microstructure analysis of the glass phase in textured cells contacted with two different pastes: (a, c) sample #T1 with paste FSP1 and (b, d) sample #T2 with paste FSP2. (a, b) Plan-view false color BSE images of the silicon metallization interface (SMI). The different colors could be assigned to different phases by qualitative SEM-EDX spectroscopy, i.e., Si pyramids (yellow squares), Ag (blue), glass phase (pink), carbon (green) and Zn-rich oxide phases (sky blue). (c, d) TEM-EDX point spectra obtained in the glass phases.

Table 2. Microstructure of glass phases in textured solar cells as well as specific contact resistance ρ_c obtained on full size (15.6×15.6 cm^2) cells using the TLM method and I-V characterization with commercial solar cell tester.

Samples	Paste	ρ_c (mΩ cm^2)	Wetting behavior of glass phase	Glass layer thickness (µm)	Ag colloid density	Ag colloid diameters / interdistances (nm)
#T1 (2129)	FSP1	21	Discontinuous	0.2-0.7	Small	5-200 / -
#T2 (2017)	FSP2	4.7	Continuous	0.07-2	Large	5-200 / -
#T3 (1004)	FSP2	5	Continuous	0.1-1	Large	10-120 / 10-30

Table 3. Quantitative chemical analysis by EDX spectroscopy in the TEM on the glass phases in textured cells contacted with paste FSP1 (sample #T1) and paste FSP2 (sample #T2).

Paste	Si (at %)	Ag (at %)	Zn (at %)	Pb (at %)	Ti (at %)	O (at %)
FSP1	26.7	4.9	8.3	12.3	1.4	46.6
FSP2	35.1	3.5	1.7	11.9	0.0	47.8

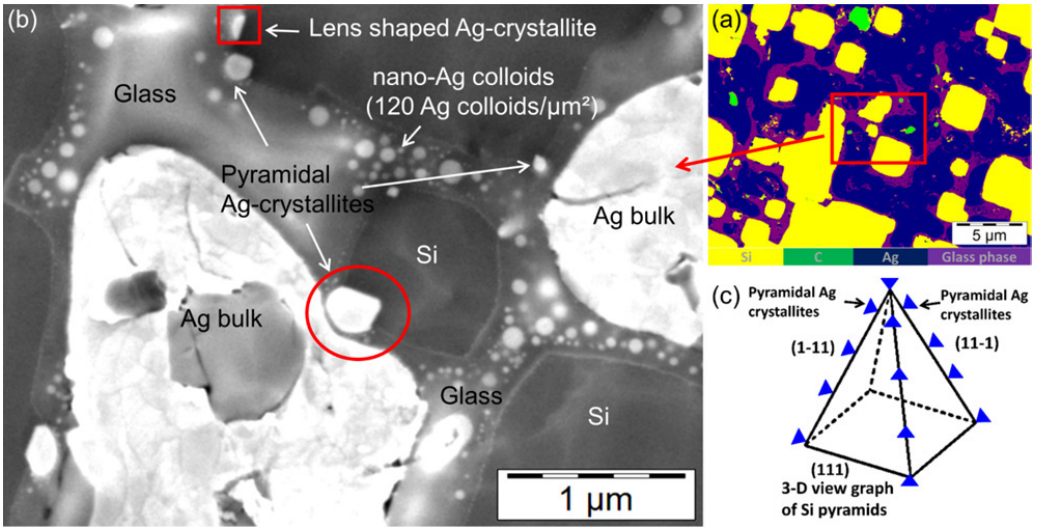

Fig. 5. (a) Plan-view false color BSE image of the silicon metallization interface (SMI) obtained on a textured cell sample #T3 contacted with FSP2. (b) Secondary electron (SE) image of section indicated in (a). (c) Schematic presentation for the preferential location of pyramidal Ag crystallites (blue diamonds) at the intersection of Si {111} planes.

3.2.2. Planar samples

Besides textured samples also planar, i.e. untextured samples, were investigated with respect to contact resistance yielding results that were not communicated so far. It was found that the contact resistance depended on the paste, as for textured samples, but also significantly on the crystallographic orientation of the Si surface. The produced cells show unprecedented low contact resistances for ⟨111⟩ oriented Si surfaces and the low contact resistances of ⟨111⟩ oriented Si surfaces has not been communicated before. Also microstructural analysis show distinct differences between ⟨111⟩ oriented surfaces and ⟨100⟩ oriented surfaces that will be outlined below. From these findings conclusions can be drawn with respect to microstructural features yielding low contact resistances. Also a discussion about the possible current path at the interface can be based on these findings. Therefore, single-crystalline solar cells with planar surfaces serve as interesting model systems for a better understanding of both (i) the microstructural features appearing at the metallization interface and (ii) the relation of these microstructural features to the contact resistance and, therefore, the current path.

Fig. 6a-c yield an overview of the different microstructures present at the SMI for samples (#P1, #P2 and #P3) and more analysis found in Table 4. Fig. 6d-f demonstrate the influence of different pastes on the microstructure and the orientation of the Si substrates on the formation of Ag precipitates.

For planar samples, paste FSP1 yielded a higher contact resistance and a discontinuous glass layer on the Si surface (Table 4) whereas paste FSP3 yielded a lower contact resistance and a continuous glass layer. The thickness of the glass layer varied from 40 to 500 nm for all the samples.

Planar cells with ⟨100⟩ oriented Si emitter yielded a higher contact resistance than ⟨111⟩ oriented Si emitters, if contacted with the same paste FSP3, as seen in Fig. 3 and Table 4.

The crystallographic orientation of the Si wafer affects the formation of Ag crystallites in direct contact with the Si emitter as well as the density of Ag colloids in the glass phase: Samples #P1 and #P2 with ⟨100⟩ oriented Si surfaces contacted with FSP1 and FSP3 revealed pyramidal as well as ellipsoidal Ag crystallites (Fig. 6a,d and 6b,e), respectively. In contrast, Sample #P3 with ⟨111⟩ oriented Si surfaces contacted with FSP3 yielded no pyramidal Ag-crystallites (Fig. 6c and 6f), only lens shaped Ag crystallites were observed. For both orientations nano-Ag colloids 50-100 nm in size were found in the glass layer. The density of Ag colloids in the glass layer was found to be significantly higher (110 Ag colloids per μm^2) in #P3 than in cells grown on ⟨100⟩ surfaces, #P1 and 2.

In the literature, the correlation of the Ag microstructure for different orientations of the Si substrate and the

contact resistance was not investigated [15, 16] or not explained properly [17]. Cabrera et al. [17] found an increase of the contact resistance of ⟨100⟩ planar Si as compared to textured, which fully agrees with our observations. However, they did not give any explanation for this increased contact resistance with respect to the microstructure. The results of Cabrera have been interpreted by others in such a way that a strong paste dependence of the contact resistance was claimed for ⟨100⟩ planar samples. We do not believe that this conclusion is right: if the ratio of the contact resistances of textured vs. planar samples is considered, the effect of paste on this ratio is only about a factor of 2. It just indicates that the effect of paste is small (factor of 2) and the effect of Si surface orientation is the dominant quantity setting the ratio of the contact resistance of planar ⟨100⟩ oriented vs. textured cells with {111} faces between 12.5 and 25.

Our microstructural analysis on 5 different planar cells processed with three different pastes (3 cells ⟨100⟩ oriented, 2 cells ⟨111⟩ oriented) confirmed the results shown in Fig. 6: the orientation of the Si determines the microstructure of Ag nanocrystals, whether pyramidal Ag crystallites are formed. On ⟨111⟩ Si Ag pyramidal crystallites were not found for any of the pastes. The surface orientation strongly affects the formation of Ag crystallites because (111) planes are close packed and, therefore, very specific planes in the crystal structure of Si.

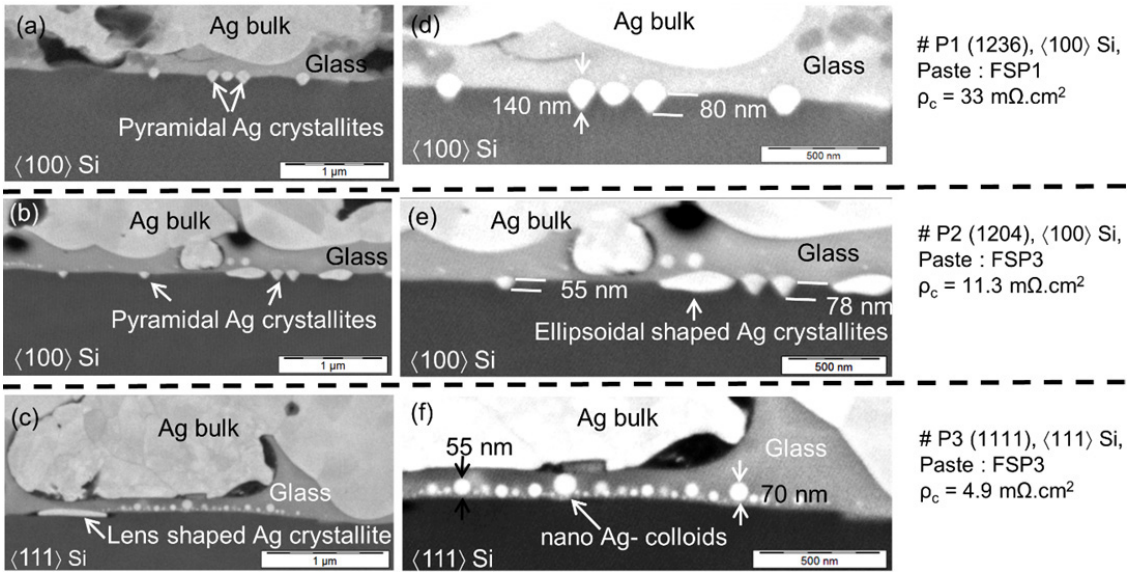

Fig. 6. Cross-sectional BSE images of the SMI obtained on the planar samples using ⟨100⟩ and ⟨111⟩ oriented Si substrates and contacted with pastes FSP1 and FSP3. Low magnification BSE images (Fig. 6a-c) and corresponding high magnification images (Fig. 6d-f).

Table 4. Microstructure of glass phases and Ag crystallites in planar solar cells as well as specific contact resistance ρ_c obtained on full size (15.6×15.6 cm^2) cells using the TLM method and I-V characterization with commercial solar cell tester.

Samples	Substrate	Paste	ρ_c (mΩ cm^2)	Wetting behavior of glass phase	Ag colloid density	Pyramidal Ag crystallites	Other Ag crystallites
#P1 (1236)	Fz-Si ⟨100⟩	FSP1	33	Discontinuous	Small	Height 70-150 nm, penetration depth 50-80 nm	None
#P2 (1204)	Fz-Si ⟨100⟩	FSP3	11.3	Continuous	Small	Height 70-150 nm, penetration depth 50-80 nm	Ellipsoidal, width 200-400 nm, height 70-120 nm
#P3 (1111)	Fz-Si ⟨111⟩	FSP3	4.9	Continuous	Large	None	Lens shaped, width 600 nm, penetration depth 30-50 nm

4. Conclusions

Combined electrical and microstructural investigations on screen printed mono-crystalline industrial Si solar cells have been carried out. Microstructure analysis includes SEM and TEM analysis on length scales from 100 µm down to 10 nm and quantitative chemical analysis of the glass phase at the interface. Temperature dependent series resistance measurements are reported in a companion paper; here, contact resistance at room temperature and microstructure analyses of the contact area are summarized. Only with this approach an understanding of the contact resistance with respect to the established microstructure is possible. Such detailed analyses have not been published before on a similar number of textured and planar cells.

Textured solar cells processed with different pastes were investigated with respect to the contact resistance and the microstructure at the contact region (SMI). A continuous wetting of the Si emitter by a glass layer filled with a high density of nano Ag colloids/precipitates correlates with a low contact resistance.

For different pastes, planar cells with <111> oriented Si yielded similar contact resistance as textured cells and smaller contact resistance as compared to planar <100> oriented cells. Such low values in contact resistance have not been reported before for planar <111> oriented Si cells.

Microstructure investigations on planar cells also yielded new insights in the formation of Ag crystallites at the Si emitter surfaces. Pyramidal shaped Ag crystallites form only on planar ⟨100⟩ oriented Si surfaces. In contrast, planar ⟨111⟩ Si surfaces yielded only lens shaped Ag crystallites but no pyramidal Ag crystallites. As a consequence in textured cells, pyramidal Ag crystallites were only located at edges or intersection of {111} faces of the Si pyramids. Therefore, the formation of pyramidal Ag crystallites strongly depends on the crystallographic orientation of the Si emitter surfaces.

Ag crystals are considered by several groups to be important for low contact resistance, it is even claimed that they are the only possible current path. Our results show that pyramidal Ag crystallites were not found in planar cells with ⟨111⟩ oriented Si surfaces, however, such cells revealed the lowest contact resistances. Therefore, it is concluded that pyramidal Ag crystallites are not necessary for contacts yielding low contact resistance. Instead, lens shaped Ag precipitates together with a high density of Ag colloids in the glass layer yield low contact resistance, as found for <111> oriented Si surfaces. A glass layer containing metallic nano-Ag colloids/precipitates between Ag bulk metallization and the Si emitter would yield a percolative charge transport.

Acknowledgements

The Baden-Wuerttemberg Stiftung is gratefully acknowledged for financing within the research project "*MikroSol* (U23)".

References

[1] R. Hoenig et al., "The nature of screen printed front side silver contacts," Energy Procedia, vol. 43, pp. 27-36, (2013).

[2] M. Hilali, S. Sridharan, C. Khadilkar, A. Shaikh, A. Rohatgi, S. Kim, "Effect of glass frit chemistry on the physical and electrical properties of thick-film Ag contacts for Silicon Solar Cells," J. Electron. Mater, vol. 35, pp. 2041, (2006).

[3] S. B. Cho, H. S. Kim, J. Y. Huh, "Mechanism underlying the beneficial effect of forming gas annealing on screen-printed Ag contacts of crystalline Si solar cells," Acta Materialia, vol. 70, pp. 1-7, (2014).

[4] S. B. Cho, K. K. Hong, J. Y. Huh, H. J. Park and J. W. Jeong, "Role of the ambient oxygen on the silver thick-film contact formation for crystalline silicon solar cells," Curr. Appl. Phys, vol. 10, pp. 222-225 (2010).

[5] K. K. Hong, S.B. Cho, J.S. You, J.W. Jeong, S.M. Bea, J.Y. Huh, "Mechanism for the formation of Ag crystallites in the Ag thick-film contacts of crystalline Si solar cells," Solar Energy Materials & Solar Cells, vol. 93, pp. 898-904, (2009).

[6] G. Schubert, F. Huster, P. Fath, "Physical understanding of printed thick-film front contacts of crystalline Si solar cells- Review of existing models and recent developments," Solar Energy Materials & Solar Cells, vol. 90, pp. 3399-3406, (2006).

[7] C. Ballif et al., "Silver thick-film contacts on highly doped n-type silicon emitters: structural and electronic properties of the interface," Appl. Phys. Lett, vol. 82, pp. 1878-1880, (2003).

[8] S. Kontermann, R. Preu, G. Willeke, "Calculating the specific contact resistance from the nanostructure at the interface of silver thick film contacts on n-type silicon," Appl. Phys. Lett, vol. 99, pp. 111905, (2011).

[9] Z. G. Li et al., "Electron microscopy study of front-side Ag contact in crystalline Si solar cells," J. Appl. Phys, vol. 105, pp. 066102, (2009).

[10] Junjie. Wu and D. S. McLachlan, "Percolation exponents and thresholds obtained from the nearly ideal continuum percolation system graphite-boron nitride," Phys. Rev. B, vol. 56, pp. 1236-1248, (1997).

[11] F. Lux, "Models proposed to explain the electrical conductivity of mixtures made of conductive and insulating materials," J. Mater. Sci, vol. 28, pp. 285-301, (1993).

[12] D. Toker, D. Azulay, N. Shimoni, I. Balberg, O. Millo, "Tunneling and percolation in metal-insulator composite materials," Phys. Rev. B, vol. 68, pp. 1236-1248, (1997).

[13] R. Hoenig, A. Kalio, J. Sigwarth, F. Clement, M. Glatthaar, J. Wilde, D. Biro, "Impact of screen printing silver paste components on the space charge region recombination losses of industrial silicon solar cells," Sol Energy Materials & Solar Cells, vol. 106, pp. 7-10, (2012).

[14] B. Willsch, P. Kumar, Z. Aabdin, N. Peranio, and O. Eibl., "Series and contact resistance measurements between 80 K and room temperature for industrial solar cells," manuscript submitted at the 5th metallization workshop, 20-21.10.2014, Konstanz, (2014).

[15] C. Khadilkar, S. Sridharan, D. Gnizak, T. Pham, S. Kim, and A. Shaikh, "Effect of glass chemistry and silicon orientation on the front contact microstructure formation in a silicon solar cell," in Proc. 20th EC PVSEC, Barcelona, Spain, pp. 1291–1296 (2005).

[16] B. M. Boyerinas, J.M. Balsam, H.A. Bruck, and A. L. Roytburd., "Effect of oxygen environment on formation of modulated Ag nanostructures along the interface of a Ag-Si heterostructure," J. Appl. Phys, vol. 113, pp. 184302, (2013).

[17] E. Cabrera, S. Olibet, J. Glatz-Reichenbach, R. Kopecek, D. Reinke, G. Schubert., "Experimental evidence of direct contact formation for the current transport in silver thick film metallized silicon emitters," J. Appl. Phys, vol. 110, pp. 114511, (2011).